RESEARCH ARTICLE

New Road Hazard Classification Enabled by Rack Force Estimation of Electric Power Steering Systems

HEE-BEOM LEE[1], HO-JONG LEE[2], DOO-HYUN LEE[3], KYUNG-JIN KIM[4], AND GI-WOO KIM[3], (Member, IEEE)

[1]Global R&D Center, HL Mando, Pangyo, Seongnam-si 13486, South Korea
[2]R&D Center of HanKook Tire, Daejeon 34111, South Korea
[3]Department of Mechanical Engineering, Inha University, Incheon 22212, South Korea
[4]The Test and Certification Technology Department, Korea Automotive Technology Institute, Cheonan-si 31214, South Korea

Corresponding author: Gi-Woo Kim (gwkim@inha.ac.kr)

ABSTRACT This study presents a preliminary investigation of a new strategy for detecting and classifying road hazards, such as potholes and bumps, based on rack force estimation of electric power steering (EPS) systems. The numerous studies on road hazard detection have primarily focused on computer-vision systems, including cameras or light detection, and ranging and vertical vibration signals measured by accelerometers mounted on suspension systems. However, conventional methods are prone to reduced accuracy owing to their susceptibility to vibrations transmitted from road surfaces to vehicles. Accordingly, considerable room for detection accuracy improvement remains. Herein, we explore a novel approach that leverages the steering rack force generated in the EPS system, considering that potholes and bumps induce vertical and lateral forces on the tire's contact patch, resulting in a net force generated by such tire moments on the vehicle steering rack. We propose an algorithm that uses an improved Kalman filter (KF) with an unknown input, combining the capabilities of a conventional KF with a disturbance observer. This algorithm aims to estimate the rack force by utilizing measurements of the steering torque and angle inputs. The estimated rack force provides features that serve as the basis for classifying road hazards. The classification performance was evaluated using metrics calculated from confusion matrix, such as accuracy, precision, recall, and F1. The proposed road hazard detection and classification algorithm was not only rigorously simulated using SIMULINK® with CarSim® software, but also is experimentally validated through in-vehicle tests.

INDEX TERMS Rack force, electric power steering system, road hazard, Kalman filter with unknown input, support vector machine, in-vehicle test.

I. INTRODUCTION

Road hazards encompass various dangers encountered while driving: unexpected potholes, illegal speed bumps, road imperfections, manhole covers, etc. Road hazard detection and classification that distinguishes road hazards from normal roads has drawn considerable research interest in recent years because road hazard detection and classification plays a

The associate editor coordinating the review of this manuscript and approving it for publication was Jad Nasreddine.

key role in vehicle chassis control and vehicle driving safety, including autonomous vehicle technology [1]. Accordingly, road hazard detection and classification technology has been the emerging subject of recent research to obtain valuable information on road conditions (i.e., road databases for cloud server systems). In particular, potholes are dangerous road hazards resulting from uneven road wear and transient weather conditions, and have consistently posed a significant risk to drivers over the last few decades [2]. The impact of potholes induces an unequal adhesion between the two

sides of a wheel, causing path deviation and roll instability. This discrepancy often leads to tire failure and compromises key automotive components such as suspension systems [3]. Therefore, the timely detection of potholes is imperative to enhance both the comfort and safety of vehicles.

Typically, potholes are detected using three-dimensional (3D) image processing technology, which involves analyzing the depth and width of these road defects. This process converts the road surface into a 3D image using a stereo vision-based camera and laser scanners [4], and is called active safety (preemptive measures to reduce the probability of damage). Conversely, a two-dimensional (2D) image-based detection method recognizes the textures and characteristics of potholes based on road surface images acquired using only a camera. This method can prevent or mitigate potentially dangerous situations [5]. However, conventional image-based methods are prone to reduced accuracy owing to their susceptibility to vibrations transmitted from road surfaces to vehicles [6]. In addition, incorporating cameras and light detection and ranging (LiDAR) sensors increases the algorithmic complexity and computational cost, especially when their functionality is extended to include pothole detection. Furthermore, while vision-based methods excel at distinguishing and locating potholes, they cannot extract physical information, such as disturbance force, moments, which are essential for vehicle control systems to respond effectively when encountering potholes.

By contrast, vibration-signal-based methods employ acceleration sensors to detect potholes by directly sensing the vehicle's impact response; this is called passive safety (reactive measures to reduce the severity of damage). Numerous studies have utilized accelerometers mounted on the sprung mass of vehicle suspension systems, aiming not only to detect potholes but also to classify and distinguish them from other potential hazards, including illegal speed bumps [7]. Threshold-based approaches aim to identify and categorize road irregularities by examining instances in which the signals obtained from inertial sensors exhibit significant alterations in the amplitude, root mean square (RMS), or crest factor and surpass predefined thresholds [8].

Other extended studies focusing on detecting and classifying road surface anomalies have endeavored to extract time or frequency-domain features from accelerometer or gyroscopic data. These features are then integrated with learning-based methods, including support vector machine (SVM), decision trees, and multilayer perceptron models [9]. Such learning-based techniques, in combination with time-domain features extracted from acceleration data, can considerably reduce the computational burdens in model generation and validation processes compared to deep learning-based methods without feature extraction. However, a critical drawback is the substantial influence of road roughness profiles on the acceleration of the sprung mass, as illustrated in Figure 1 (b).

This poses a challenge in capturing signature signals and establishing suitable thresholds for pothole detection.
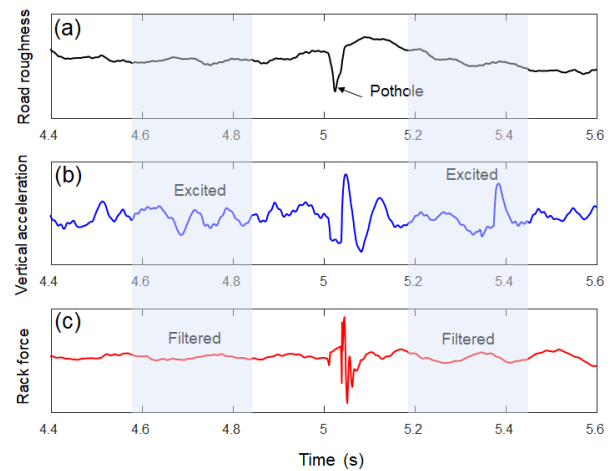

FIGURE 1. Signal signature comparison at 30 km/h straight driving: (a) Road roughness (profile) with a sudden pothole, (b) Corresponding vertical acceleration of the vehicle suspension systems, and (c) Rack force of the EPS system.

Moreover, other factors, such as roll and pitch motions during steering maneuvers, and suspension damping, can further the impact sprung-mass acceleration [10]. Recently, accelerometers (G-sensor) have been implemented in steering systems, such as steering columns, rather than suspension systems, and demonstrated notable advantages for pothole detection [11]. Despite the enhanced sensitivity, utilizing acceleration data directly from the steering system presents difficulties, owing to potential interference from numerous factors, such as noise and vibrations originating from other vehicle components [12]. Nevertheless, the steering system holds promise as a more viable alternative for effective pothole detection.

Recently, automotive tire manufacturers have attempted to detect road pothole using smart tire sensor technology. Road condition information detected by smart tire sensors can be shared through a cloud server when the lead vehicle encounters a pothole, as depicted in Figure 2. This approach seems promising because subsequent vehicles can use this shared information to navigate and avoid road hazards such as potholes, potentially reducing computational demands and enhancing efficiency. Since the tires are the only components of the vehicle system in direct contact with the road surface, they inherently possess a high potential for detecting road hazards. However, smart tire sensors have technical issues. They typically have low sampling frequencies (e.g., 1 Hz). Given the vehicle's velocity (e.g., 14 m/s or 50 km/h), this low sampling frequency is unsuitable for road hazard detection.

Moreover, high-frequency sensors based on smart tires, developed to address this issue, face challenges in commercialization because of battery-life and durability concerns. The sensor fusion-based indirect method can be an effective supplementary system for smart tire sensors or act as a fail-safe system where smart tire sensors may not function properly. The sensor fusion-based indirect method functions
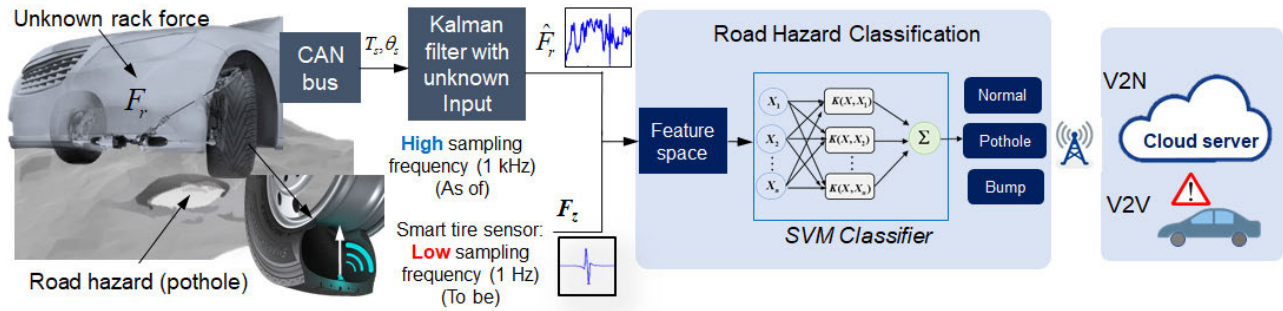
FIGURE 2. Schematic overview of the proposed road pothole detection method using both proof-of-concept smart tire sensor built-in pneumatic tires (direct) and sensor fusion-based rack force estimation in the EPS system (indirect method).

through the control area network (CAN) bus. It is currently utilized in various real-time vehicle control systems with a relatively high sampling frequency (e.g., 1 kHz). This indirect method can enhance the accuracy of road hazard detection in situations in which smart tire sensors are limited.

Electric power steering (EPS) systems, also referred to as motor-driven power steering (MDPS) systems, have been developed to assist drivers and reduce steering effort [13]. These steering control systems are designed to improve the vehicle's ride and handling performance by compensating for external disturbances, providing drivers with a road feel, and accommodating irregularities in road surface profiles [14]. Uneven road surfaces exert vertical and lateral forces on the tire's contact patch, generating moments around the kingpin axis [15]. The net force generated by the tire moments on a steering rack of a vehicle (frequently referred to as the rack force) encompasses the interaction between the road surface and the tire, which is heavily influenced by road profiles [16]. Naturally, rack force estimation is still useful for detecting road irregularities. Thus, a more advantageous approach would involve a simpler and more intuitive solutions. In addition, rack force estimation offers higher robustness and sensitivity compared to conventional method, such as computer vision, and it provides better accuracy by reducing noise contamination compared to smart tire sensors. Moreover, the proposed method utilizes the KF-UI based on a dynamic model to accurately estimate rack force in EPS systems, providing precise and low-latency compared to the response type such as the use of accelerometer. Yang et al. [17] previously employed an extended Kalman filter with an unknown input (EKF-UI) to estimate unknown earthquake inputs. The EKF-UI successfully estimated the unknown earthquake input and state variables under nonlinear structural dynamics. Similarly, a KF-UI was applied to estimate both state variables and unknown road roughness inputs for a full-car vehicle suspension model [18]. This algorithm was modified and generalized for application to a general linear system called the KF-UI [19].

Despite the numerous research concerning road hazard detection, primarily focusing on computer vision systems

including cameras or light detection and ranging and vertical vibration signals measured from accelerometers mounted on suspension systems or inertial measurement unit (IMU), considerable room for detection accuracy improvement remains. Furthermore, although previous studies have shown some promising results in detecting road hazards such as potholes, the following issues should be further considered.

- Although computer vision-based active methods using a camera module and a LiDAR are preemptive measures to reduce the probability of damage, they entail a substantial computational burden owing to image processing demands. In addition, they are still highly sensitive to weather and lighting conditions, necessitating the deployment of high-performance cameras, which costs to obtain detailed road surface information including road hazards.
- Because conventional methods based on vehicle acceleration signals suffer from the substantial influence of road roughness profiles, as illustrated in Figure 1 (b), this disadvantage poses a challenge in capturing signature signals and establishing suitable thresholds for road hazard (e.g. potholes) detection. The excitation effects of normal road surface characteristics (texture wavelength, 10 mm $\sim$ 100 mm) should be removed or minimized for robust detection of road hazards.

To overcome abovementioned drawbacks, we explore a novel approach leveraging the steering rack force generated in the EPS system considering that potholes and speed bumps induce both vertical and lateral force on the tire's contact patch, resulting in a net force generated by such tire moments on the steering rack of a vehicle. Because this rack force acts in the lateral direction, our approach can minimize the effects of normal road surface characteristics (vertical excitation). Although some studies have shown that it is possible to achieve the new method for the rack force estimation [14], there were no reports that rack force estimation responses can be used to signature signals for road hazard classification. For road hazard classification, the classification accuracy also should be considered. However, most previous study on the road hazard classification have shown the highest accuracy of 88.8 % [9].

Therefore, the objective of this study is to develop a new road hazard detection and classification method based on rack force estimation insensitive to normal road surface characteristics, and combines with learning-based SVM model to achieve the enhanced accuracy of 90 % (research goal). SVM classifier model will use key features extracted from an estimated rack force (unknown disturbance input) produced in an EPS system. The use of SVM model leverages its advantages in handling high-dimensional data, preventing overfitting, and performing nonlinear classification. The remainder of this paper is organized as follows. Section II outlines the KF-UI algorithm designed to estimate the unknown rack force input, and the SVM model for road hazard classification. Section III presents the experimental validation of the proposed method using in-vehicle test with SVM-based classification. Section IV presents our conclusions and future work.

II. DESIGN OF RACK FORCE ESTIMATOR

A. TIRE AND ROAD MODELS

All the input data utilized for the simulation and training were simulated from a sedan vehicle model at a driving speed of 40 km/h using CarSim®(V 9.0) [20]. Properly selecting the tire model is important for accurately estimating the rack force because it substantially influences the tire force generation. For this preliminary investigation, the empirical Pacejka tire model (often called the magic formula) was employed with standardized model coefficients to represent the visco-elastic properties of the tires [21]. The tire forces and moments were derived from kinematic variables, including the lateral slip angle, longitudinal slip ratio, inclination angle, and tire vertical deflection defined by the spatial relationship between the wheel and contact centers under steady-state conditions. Notably, the static relationship between the tire vertical deflection of the tire and the vertical load (force) is nonlinear because the matrix of a pneumatic tire is a polymer (i.e., rubber), as shown in Figure 3 (b). This static tire model is then extended to include transient behavior using a separate filter to account for tire lag [28].
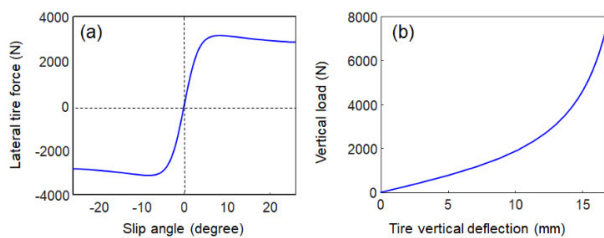
FIGURE 3. Characteristics of the Pacejka tire model (a) Slip angle vs. lateral tire force (b) Vertical load vs. tire deflection curve.

A parallel-track road model was used to synthesize the road elevation (i.e., road roughness and profile) on the left and right tracks for the road-roughness model. The data regarding the vehicle responses to the synthesized road input were continuously collected. The road elevation was modeled
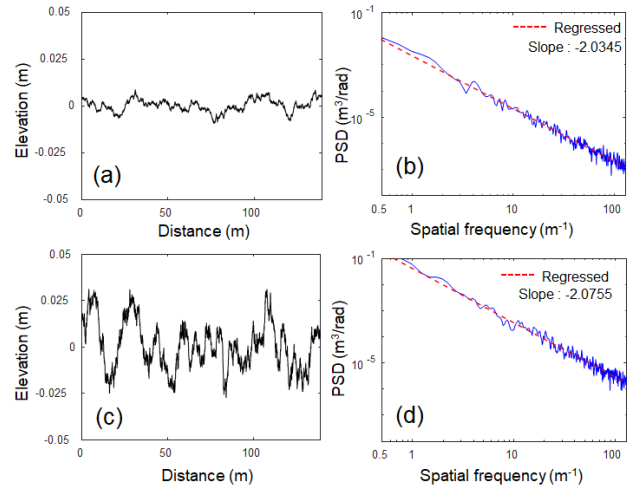
FIGURE 4. Road roughness and its corresponding PSD curve for (a), (b) an A-class road (smooth) and (c), (d) a C-class road (rough).

based on the ISO 8608 standard where the international roughness index classifies roads based on the different levels of their power spectral density (PSD) functions [22]. This study synthesized the road roughness for both A-class and C-class roads, as illustrated in Figure 4. The calculated PSD function, determined using Welch's method, revealed linear regression with slopes of -2.0345 and -2.0755 respectively, close to the ISO-defined value of -2 (ideal). Potholes are typical road defects that can be classified based on shape and size. The most representative mathematical model of the pothole was implemented in the simulation, as showcased in Figure 5. The potholes can be modeled as a square wave pulse which can be represented as.

$$r(\theta) = \begin{cases} -\alpha & |\theta| \leq \dfrac{\beta}{2} \\ 0 & |\theta| > \dfrac{\beta}{2} \end{cases} \quad (1)$$

where $\alpha(0.2 \text{ m})$ and $\beta(50 \text{ mm})$ represent the pothole depth and width respectively [23].
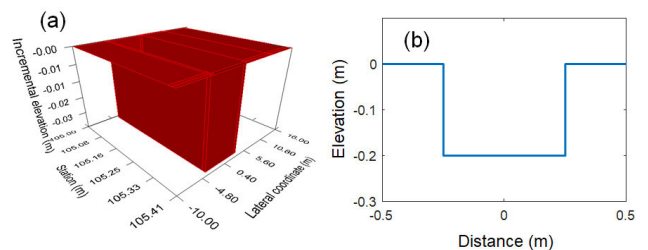
FIGURE 5. Geometric model of the pothole ($\alpha = 20$mm, $\beta = 0.5$m) (a) 3D view (b) Cross-sectional view.

B. DYNAMIC MODEL OF THE EPS SYSTEM

In this study, a rack-type EPS system is represented as a reduced-order model with two degrees of freedom (DOF), as shown in Figure 6. The EPS system can be represented
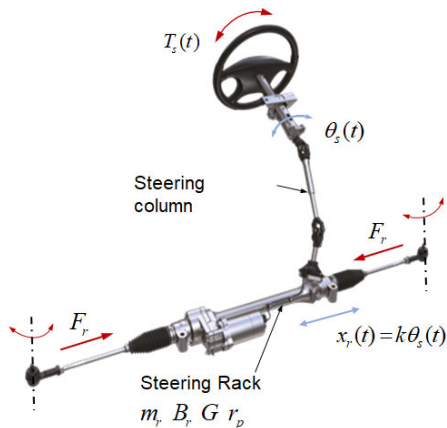
FIGURE 6. Schematic illustration depicting the EPS system (R-MDPS type).

by two lumped inertias: the steering wheel column and the rack combined with pinion and the electric motor. These two inertias are connected by a stiff torsion bar spring that facilitates the movement of the system as a whole [24]. Although an actual steering system possesses a complex kinematic linkage structure, the proposed model effectively captures its dynamic behavior and has been experimentally validated in numerous studies. To maintain the model simplicity associated with the algorithm design, the assistant torque was assumed to be negligible for this study, given its easy measurement and straightforward incorporation into the model by merely adding the corresponding amount of assist torque. The governing equations of the EPS system are formulated as follows [25]:

$$J_s\ddot{\theta}_s + K_s\left(\theta_s - \frac{x_r}{r_p}\right) + d_s\dot{\theta}_s = T_s \qquad (2)$$

$$M_r\ddot{x}_r + d_r\dot{x}_r = \frac{G}{r_p}K_s\left(\theta_s - \frac{x_r}{r_p}\right) + F_r \qquad (3)$$

where θ_s represents the steering-wheel angle, x_r denotes the lateral displacement of the rack; and T_s and F_r represent the steering torque and rack force respectively.

The steering-wheel torque applied by the driver is transmitted through a torsional bar that connects the steering column to the rack and pinion module which has an equivalent mass and damping coefficient d_r. G represents the transmission ratio of the reduction mechanism and r_n denotes the radius of the steering pinion. Eq. 3 (the rack module) can be simplified and reformulated by assuming a linear relationship between the rack displacement and steering angle:

$$J_r\ddot{\theta}_s + D_r\dot{\theta}_s = GT_s + r_pF_r. \qquad (4)$$

The state equation can then be expressed as follows:

$$\dot{x} = A_cx + B_cu + B_c^*u^*, \qquad (5)$$

where

$$A_c = \begin{bmatrix} 0 & 1 \\ 0 & -\frac{D_r}{J_r} \end{bmatrix} \quad B_c = \begin{bmatrix} 0 \\ \frac{G}{r_pJ_r} \end{bmatrix} \quad B_c^* = \begin{bmatrix} 0 \\ \frac{1}{J_r} \end{bmatrix} \qquad (6)$$

TABLE 1. Parameters for the EPS model.

Symbol	Parameter	Value
J_r	Moment of inertia of steering rack	$0.02 \text{ kg}m^2$
D_r	Damping coeff. of the steering rack	642 N s/m
G	Reduction gear ratio	17
r_p	Pinion radius	0.0085 m

$$x = \begin{bmatrix} \theta_s & \dot{\theta}_s \end{bmatrix}^T , \quad u = T_s , \quad u^* = F_r. \qquad (7)$$

To design the KF-UI, a continuous-time system model (Eq. (5)) was discretized using Euler's method, as follows:

$$\begin{aligned} x_{k+1} &= (I + t_sA_c)x_k + t_sB_cu + t_sB_c^*u^* \\ &= Ax_k + Bu + B^*u^* \end{aligned} \qquad (8)$$

where t_s is the sampling time (10 ms in this study); the asterisk (*) represents the unknown input. The measurement equation is expressed as follows:

$$z_k = Cx_k + Du_k + D^*u_k^*, \qquad (9)$$

where

$$C = \begin{bmatrix} 1 & 0 \\ 0 & -\frac{D_r}{J_r} \end{bmatrix} \quad D = \begin{bmatrix} 0 \\ \frac{G}{r_pJ_r} \end{bmatrix} \quad D^* = \begin{bmatrix} 0 \\ \frac{1}{J_r} \end{bmatrix} \qquad (10)$$

$$z_k = \begin{bmatrix} \theta_s & \ddot{\theta}_s \end{bmatrix}^T \qquad (11)$$

The steering wheel angle and torque controlled by the driver can be measured by a torque angle sensor mounted on contemporary EPS systems. In Eq. (11), the angular acceleration is obtained by taking the second derivative of the steering wheel angle. The physical parameters of the EPS system model used in the simulation are listed in Table 1.

C. KF-UI

This section introduces the KF-UI algorithm for an EPS system, which simultaneously estimates the unknown rack force and state variables. The state-space model expressed in Eqs. (5) and (9) can be rewritten as

$$\begin{aligned} x_{k+1} &= Ax_k + Bu_k + B^*u_k^* + w_k \\ z_k &= Cx_k + Du_k + D^*u_k^* + v_k, \end{aligned} \qquad (12)$$

where w_k represents a system-noise vector, and v_k denotes the measurement-noise vector. Upon solving the optimization problem and conducting linear algebra operations, the recursive solution of the KF-UI is derived as follows [19]:

1) INITIAL ESTIMATION

$$\hat{x}_{0|0} = E[x_0], \quad \hat{u}_0^* = E[u_0^*]$$

$$P_{0|0} = E\left[(x_0 - \hat{x}_{0|0})(x_0 - \hat{x}_{0|0})^T\right]$$

$$S_0 = E\left[(u_0^* - \hat{u}_0^*)(u_0^* - \hat{u}_0^*)^T\right] \qquad (13)$$

2) PREDICTION

$$\hat{x}_{k+1|k} = A\hat{x}_{k+1|k} + Bu_k + B^*\hat{u}_k^*$$
$$P_{k+1|k} = AP_{k|k}A^T + Q \tag{14}$$

3) KALMAN-GAIN CALCULATION

$$K_{k+1} = C^T P_{k+1|k}(CP_{k+1|k}C^T + R)^{-1} \tag{15}$$

4) UNKNOWN INPUT ESTIMATION

$$S_{k+1} = [D^{*T}R^{-1}(I - CK_{k+1})D^*]^{-1}$$
$$\hat{u}_{k+1}^* = S_{k+1}D^{*T}R^{-1}(I - CK_{k+1})(z_{k+1} - C\hat{x}_{k+1|k} - Du_k) \tag{16}$$

5) CORRECTION

$$\hat{x}_{k+1|k+1} = \hat{x}_{k+1|k} + K_{k+1}(z_{k+1} - C\hat{x}_{k+1|k} - Du_k - D^*\hat{u}_{k+1}^*)$$
$$P_{k+1|k+1} = (I + K_{k+1}D^*S_{k+1}D^{*T}R^{-1}C)(I - K_{k+1}C)P_{k+1|k} \tag{17}$$

At $k = 0$, the filter is initialized with the initial condition expressed in Eq. (13), wherein $E[\cdot]$ represents the ensemble average of a random variable. At the kth step, *a priori* state estimate $\hat{x}$ and *a priori* covariance matrix $P_{k+1|k}$ are predicted from the system model using Eq. (14). The optimal Kalman gain K_{k+1} is then calculated using Eq. (15).

Next, the unknown input $\hat{u}_{k+1}^*$ and its covariance S_{k+1} are estimated based on the measurement z_k through Eq. (16). Finally, *a posteriori* state estimate $\hat{x}_{k+1|k+1}$ and its covariance matrix $P_{k+1|k+1}$ are corrected using Eq. (17) by employing the measurement information. The results computed at the kth step are reused, as the KF-UI recursively estimates the next step. The KF-UI and conventional KF algorithms share the same structure during the prediction and Kalman-gain calculation stages, as shown in Eqs. (14) and (15). This implies that unknown inputs do not influence the *a priori* estimation or Kalman gain. However, while an unknown-input estimation stage exists in the KF-UI, it is absent in the conventional KF. This is because the KF-UI algorithm can estimate the unknown input, introducing a difference during the correction stage. The additional term $(I + K_{k+1}D^*S_{k+1}D^{*T}R^{-1}C)$ represents the results of the unknown input. It is multiplied when estimating *a posteriori* covariance matrix $P_{k+1|k+1}$ in the KF-UI algorithm, not in the conventional KF algorithm. The following two conditions should be satisfied in the system to ensure the successful estimation of both the unknown input and state variables:

$$B^* \neq 0, \ D^* \neq 0 \tag{18}$$
$$m > q. \tag{19}$$

Equation (18) implies that the state-measurement equation represented by Eq. (12) necessitates the inclusion of an unknown input, $\hat{u}_k^*$. Because $D^* \neq 0$ signifies that the measurement equation should include the unknown input
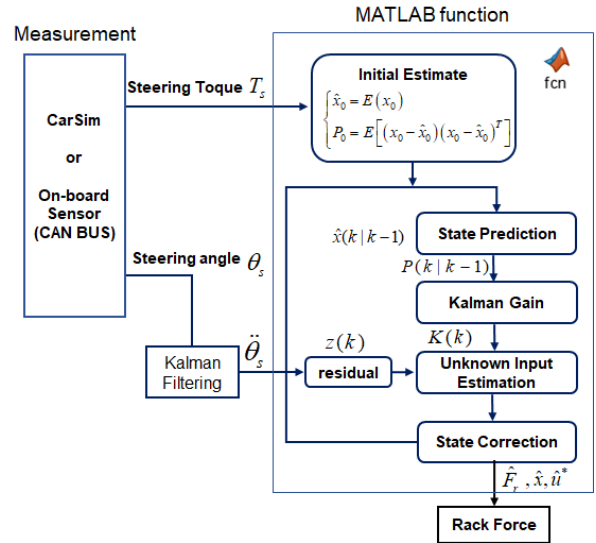

FIGURE 7. Comprehensive flowchart depicting the rack force estimation.

$\hat{u}_k^*$, it can serve as a constraint when selecting sensors for implementing the KF-UI algorithm. This condition can be fulfilled by obtaining the steering angle acceleration, a non- critical factor in the steering system. Additionally, the second condition (Eq. (19)) indicates that the number of measurements (m) must exceed the number of unknown inputs (q). Failure to satisfy this condition makes the system unobservable, preventing the KF-UI from estimating unknown inputs.

In addition to these two conditions, ensuring the system's observability is crucial when designing the measurement equation. In the rack force estimation problem, an absolute angle (e. g., steering angle or rack displacement) is required to satisfy the observability condition. In other words, the observability matrix must have full rank because the rack force estimation fails unless the system is observable. This is also significant for road roughness and state estimation based on the KF-UI. Consequently, a careful selection of the measurements (Eq. (11)), particularly the sprung mass displacement, is essential for the KF-UI algorithm to operate properly. The system-noise covariance matrix Q and measurement-noise covariance matrix R in Eqs. (14) and (15), respectively, can be defined as

$$\begin{cases} E[w_k] = 0 \\ E[w_k w_k^T] = Q \end{cases}, \quad \begin{cases} E[v_k] = 0 \\ E[v_k v_k^T] = R \end{cases} \tag{20}$$

where w_k and v_k are zero-mean white Gaussian noise with covariance Q and R, respectively. These two equations hold for both the conventional KF and KF-UI. Therefore, the Q and R matrices of the KF-UI can be designed for a conventional KF. The overall flowchart of the adaptive extended KF-UI (AEKF-UI) algorithm is illustrated in Figure 7. Using CarSim software [20], the typical simulation results for straight and sinusoidal driving scenario using are compared and illustrated in Figure 8.
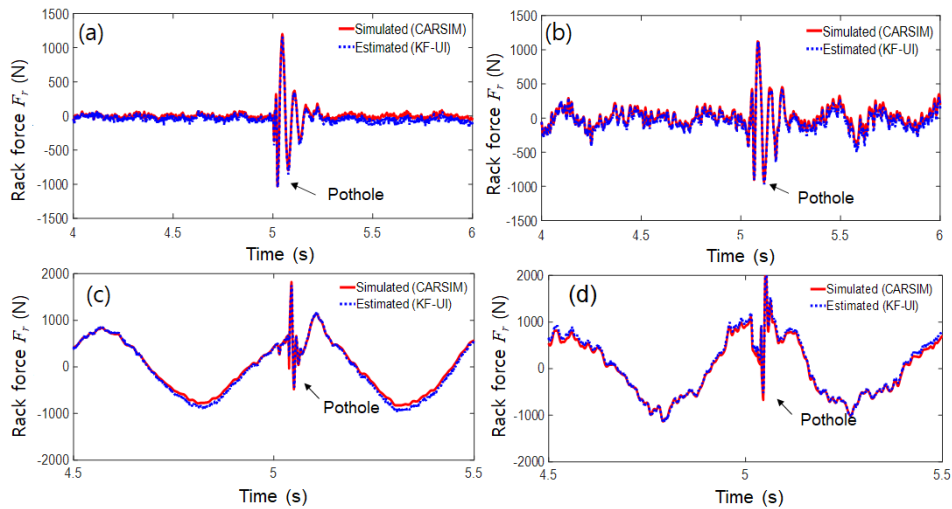
FIGURE 8. Comparison of simulated and estimated rack force responses (30km/h) (a) and (b) Straight driving, and (c) and (b) Sinusoidal, (a) and (c) A-class road, (b), (d) C-class road.

Notably, the rack force estimation using KF-UI (simulated) successfully tracked the CarSim model. The distinct peaks attributed to potholes are easily reflected in features derived from the rack force response. This feature set was capable of capturing the variations between different types of road anomalies and normal roads.

FIGURE 9. (a) Pothole (b) 760 × 730 mm, depth = 20 mm, (c) 760 × 730 mm depth = 40 mm, (d) bump 2000 × 2000 mm, depth = 75 mm.

III. PERFORMANCE VALIDATION
A. IN-VEHICLE TEST SET-UP
The in-vehicle test system, depicted in Figure 9, was designed to validate the proposed algorithm. It comprises a ground electric vehicle (model: Hyunndai IONIQ5) and data acquisition devices. The on-board sensor signals are acquired from the controller area network flexible data-rate (CAN FD) communication bus. To facilitate this communication protocol, a compact CAN FD interface device (model: Kvaser) and CANoe software (Vector Informatik GmbH) are used. The vehicle was driven straight at three different speeds: 20, 30, and 40 km/h. Additionally, bumps with heights of 75 mm and potholes with depths of 20, 30,

and 40 mm were included. Various load conditions and tire pressures were also considered, resulting in a total of 155 driving scenarios for in-vehicle tests. The only two measurement signals (steering angle generated by the driver and steering torque input) were extracted and post-processed (resampling).
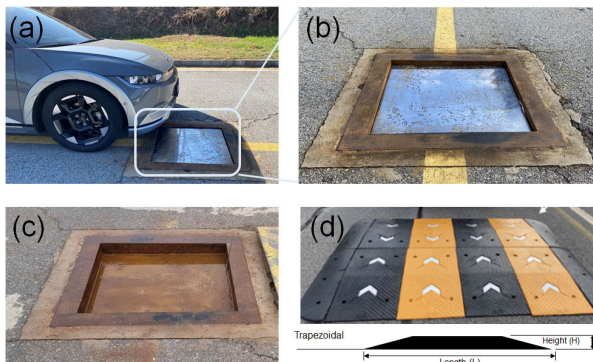
B. SYSTEM IDENTIFICATION OF THE EPS MODEL
In this study, the recursive least squares estimator (RLSE) was adopted to identify unknown parameters in the vehicle's EPS system. Because the performance of the rack force estimator largely depends on the accuracy of the model parameters, an offline system identification process was required. To design the RLSE, the steering system model (Eqs. (4) and (5)) is reformulated in matrix form as

$$y_k = h_k^T \theta_k + v_k \tag{21}$$

where

$$y_k = T_s h_k^T = \begin{bmatrix} \ddot{\theta}_s & \dot{\theta}_s \end{bmatrix} \theta_k = \begin{bmatrix} J_r & D_r \end{bmatrix}^T, \tag{22}$$

The system is represented by a linear model in the form of Eq. (21), where y_k denotes the output vector, and h_k^T represents the measurement matrix; these are known values that can be obtained by processing sensor signals. θ_k denotes the unknown parameter vector to be estimated. It includes J_r and B_r, which represent the moment of inertia of the steering rack and the damping coefficient respectively. v_k signifies measurement noise. The numerical values for y_k and h_k^T were directly measured using the CAN data. To complete the measurement matrix (Eq. (11)), the steering angular acceleration $\ddot{\theta}_s$ was estimated via simple Kalman filtering of the measured steering angle θ_s without direct low-pass filtering and double differentiation [30]. The RLSE was then designed as follows [31]:

TABLE 2. Identified system parameters of steering rack.

Symbol	Parameters	Value
J_r	Moment of inertia	$0.064 \ kg \cdot mm^2$
D_r	Damping coefficient	$0.232 \ N \cdot s/m$

1) INITIAL ESTIMATES

$$\hat{\theta}_0 = E\left[\theta\right] \tag{23}$$

$$P_0 = E\left[\left(\theta - \hat{\theta}_0\right)\left(\theta - \hat{\theta}_0\right)^T\right] \tag{24}$$

2) KALMAN-GAIN CALCULATION

$$K_{k+1} = P_k \boldsymbol{h}_{k+1}\left(\boldsymbol{h}_{k+1}^T P_k \boldsymbol{h}_{k+1} + \boldsymbol{w}_{k+1}^{-1}\right)^{-1} \tag{25}$$

3) PARAMETER UPDATE

$$\hat{\boldsymbol{\theta}}_{k+1} = \hat{\boldsymbol{\theta}}_k + K_{k+1}\left(\boldsymbol{y}_{k+1} - \boldsymbol{h}_{k+1}^T \hat{\boldsymbol{\theta}}_k\right) \tag{26}$$

4) COVARIANCE UPDATE

$$P_{k+1} = \left(I - K_{k+1}\boldsymbol{h}_{k+1}^T\right) P_k \tag{27}$$

In the first step, the estimated parameter and its covariance are initialized to arbitrary values as they are usually unknown. The estimated parameter vector is then calculated by Eqs. (24), (25), and (26), updating each time step in a recursive manner. Compared to second differentiation of steering angle signal to obtain angular acceleration, simple Kalman filtering provides an excellent estimation of the angular acceleration from the measured steering angle, as shown in Figure 10. The two parameters converging over time to a certain finite steady-state were successfully estimated, as shown in Figure 11, and are listed in Table 2.

C. RACK FORCE ESTIMATION

The typical rack force estimation responses to potholes and speed bumps were shown in Figures 12 and 13. Similar to simulation results, oscillating transient peaks were observed in all rack force estimation responses. From these experimental observations, KF-UI algorithm can effectively capture the transient peak response caused by potholes and speed bumps in the straight steering scenarios. Although the estimated rack force responses for speed bumps are lower than those for the potholes, they exhibited consistent patterns. However, peak detection method such as z-scores method must be ineffective to detect potholes (spikes) from rack force estimation because of the time-varying characteristics of rack force estimation responses, as shown in Figure 12 and 13 [24].

D. ROAD HAZARD CLASSIFICATION

In this study, rack force responses under different road conditions presented in Section III-C were utilized as a pre-trained classification model for a support vector machine
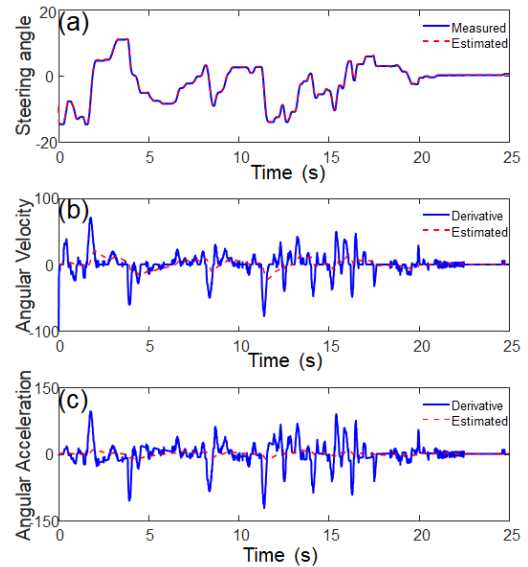

FIGURE 10. Kalman filtering of steering angle signal: (a) Steering angle, (b) Angular velocity, and (c) Angular acceleration.
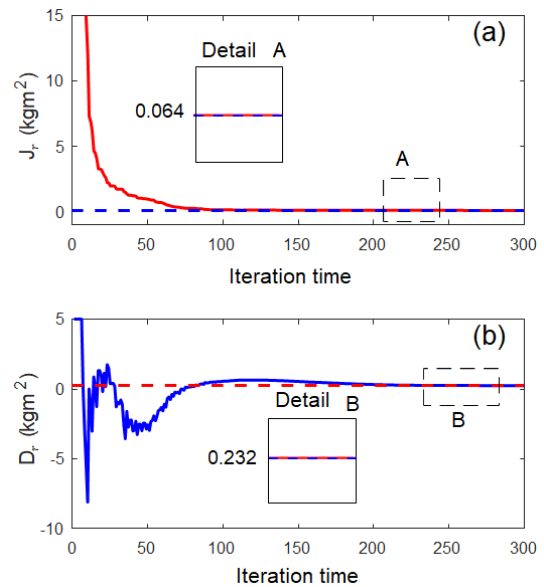

FIGURE 11. System identification results for system model (R-MDPS, IONIQ5). (a) Moment of inertia of steering rack, (b) Damping coefficient of steering rack.

(SVM) to distinguish potholes from other road hazards. The SVM, a supervised machine learning algorithm widely used for various classification and regression applications, was used to classify the road hazards where accuracy is critical because of its memory efficiency andbecause it could handle high-dimensional computations with minimal risk of malfunction, and generate hyperplanes (decision planes) with the largest margin [32]. In addition, the SVM can efficiently handle non-linear decision boundaries using a kernel trick. Typically, the SVM algorithm maps the input data into a high dimensional space using a kernel function, enabling the
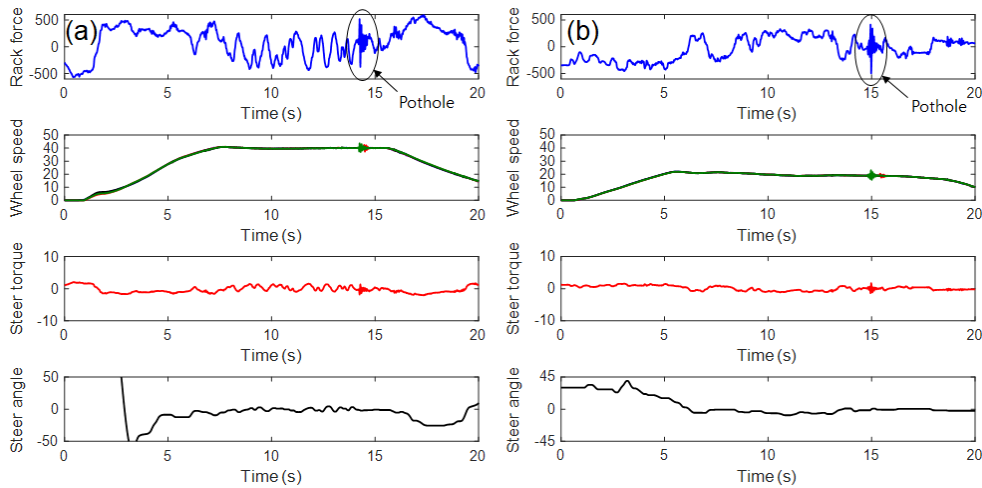
FIGURE 12. Comparison of rack force estimation (straight steering) for pothole (depth 40 mm) (a) 40 km/h, (b) 20 km/h.
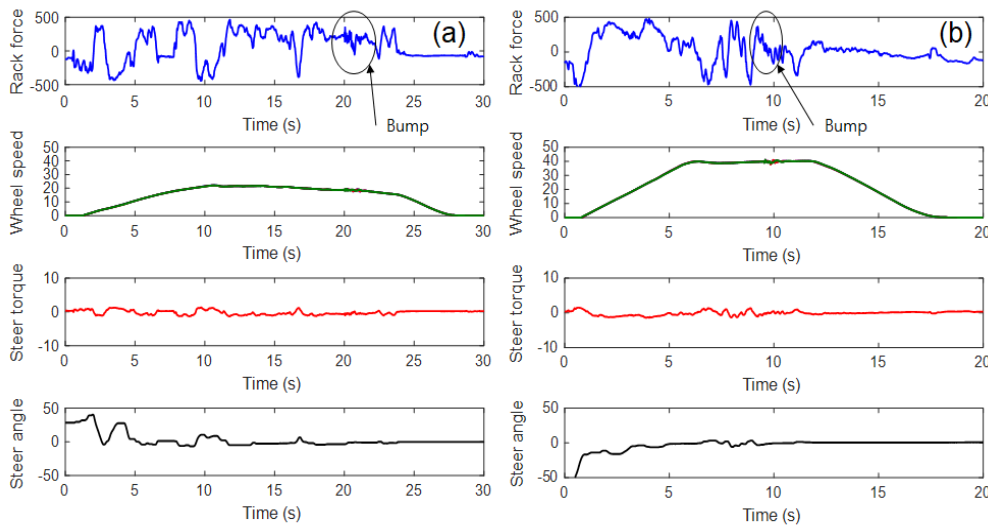

FIGURE 13. Comparison of rack force estimation (straight steering) for speed bump (a) 20 km/h, (b) 40 km/h.

algorithm to learn an optimal decision boundary (hyperplane) separating the training data into distinct multiple classes. Common kernel functions include linear, polynomial, radial basis, and sigmoid. Gaussian kernels have recently gained popularity and are often deemed more suitable for SVMs, and are defined as [33].

$$K(x_i, x_n) = \exp\left(-\frac{\|x_i - x_n\|^2}{2\sigma^2}\right) \quad (28)$$

The MATLAB/Simulink® Statistics and Machine Learning Toolbox was used for the SVM classification [34]. The SVM aims to find the hyperplane that maximizes the margin among the classes. The SVM can also classify with non-linear decisions using kernel functions, including linear, polynomial, and radial basis function (RBF) [35]. The total number of 423 datasets was partitioned into training and validation sets in the ratio of 9:1. The SVM model was trained
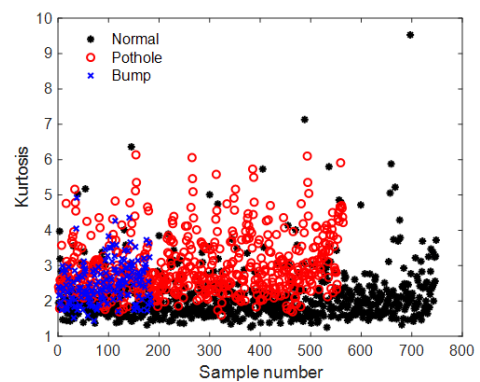

FIGURE 14. An example of feature for SVM model (kurtosis of rack force responses).

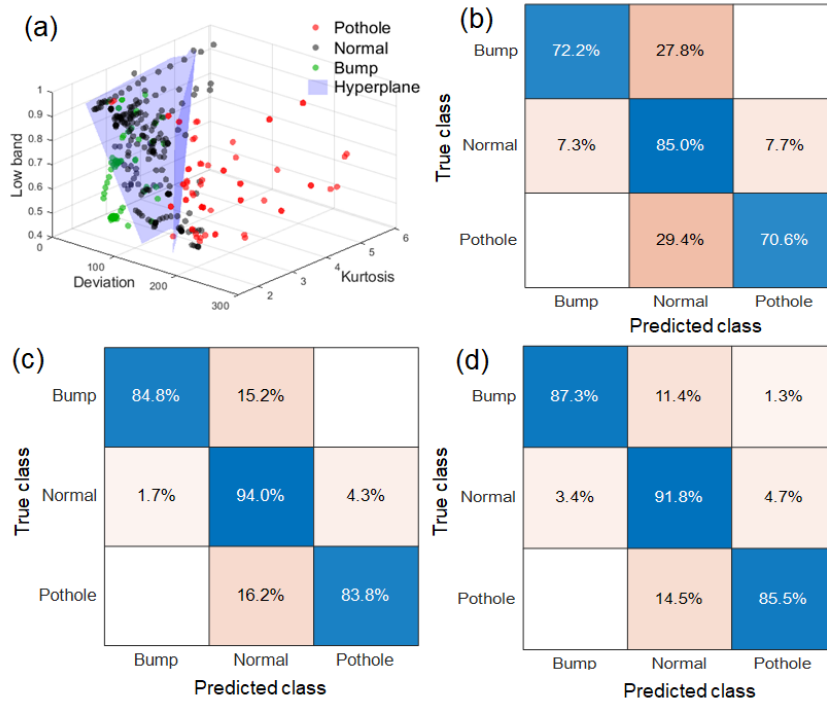to employ an RBF kernel function under CPU (14th Gen Intel®Core™i7-14700F) and a GPU (NVIDIA GeForce RTX

FIGURE 15. Road hazard classification results using confusion matrix (a) 2-D hyperplane depicting for 3-features SVM, (b) Confusion matrix for linear SVM (3-features) (c) Confusion matrix for nonlinear SVM (4-features), (d) Confusion matrix for nonlinear SVM (5-features).

4070). SVM has two hyper-parameters which are C and γ. C is a hyper-parameter to control error in SVM. When low C means low error, and large C means large error. γ decided that how much curvature we want in a boundary. When γ is high, there is more curvature in hyperplane. When γ is low, there is less curvature hyperplane. To find the best hyper parameters, a grid search with cross-validation was used, resulting in $C = 1$ and $\gamma = 10$. Before applying a machine-learning algorithm to build classification models, the data were preprocessed through feature extraction and road hazards labeling. This feature set was capable of capturing the variations between different types of road anomalies and normal roads. Road anomalies can be characterized by the mean, deviation, variance, standard deviation, root mean square, range of rack force, etc. These features facilitate the SVM model in identifying and distinguishing potholes from other road hazards. The characteristics of the rack force estimation responses (i.e. Figure 12 and 13) were qualitatively analyzed to extract the features for the classifier input. Although the rack force estimation performance was not directly evaluated by installing force sensors on the vehicle owing to hardware limitations, a similarity between the profile of the estimated rack force and the actual measured values for specific scenario scenarios was observed based on findings from previous studies [36]. The selection of effective feature from time domain and frequency domain by fast Fourier transform (FFT) was facilitated using a correlation-based feature selection technique [8]. Three features are then extracted as a baselined feature (standard deviation,

kurtosis, and FFT energy ratio - low band). For three different cases; baseline, four (skewness is added), and five features (skewness and total power are added); were compared because the classification can be improved by increasing the number of features (dimension). As shown in Figure 14, kurtosis can roughly distinguish three road conditions. Typically, the window size can help to determine the granularity or resolution of an SVM, and influences the computational complexity of the SVM. In real-time monitoring systems, a smaller window size may be preferred to detect and respond to rapid changes or anomalies promptly. Accordingly, the window size was set to be 0.5 s for the in-vehicle test.

The datasets were collected until the end of the time required to train the SVM model by computing the features for every 50 rows. Four well-known performance scores were used in the evaluation process: recall, precision, F1 score, and accuracy. The calculation formula is shown as follows:

$$Recall = \frac{TP}{TP + FN} \tag{29}$$

$$Precision = \frac{TP}{TP + FP} \tag{30}$$

$$F1\ Score = \frac{2 \times Recall \times Precision}{Recall + Precision} \tag{31}$$

$$Accuracy = \frac{TP_{normal} + TP_{pothole} + TP_{bump}}{Number\ of\ Test\ sets} \tag{32}$$

The linear SVM classifier exhibited an accuracy of 0.7974, precision of 0.7703, recall of 0.7215, and F1 score of
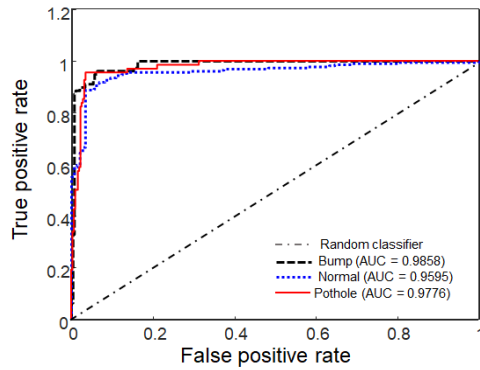
FIGURE 16. A ROC curve for nonlinear SVM (4-features).

0.7451 for the bumps. It obtained a 0.8257 precision, 0.8504 recall, and 0.8379 F1 score for normal roads. Finally, it obtained a 0.7273 precision, 0.7059 recall, and 0.7164 F1 score for the potholes. Figure 15 (c) shows the highest classification metrics of the nonlinear SVM classifier with four features, exhibiting a0.9186 accuracies, 0.9103 precision, 0.8987 recall, and 0.9045 F1 score for bumps. A precision of 0.9397, recall of 0.9316, and F1 score of 0.9356 were obtained for normal roads. Finally, it obtained a 0.8592 precision, 0.8971 recall, and 0.8777 F1 score for the potholes. Figure 15 (d) shows the nonlinear SVM classifier with five features, showing a 0.8766 detection accuracy, 0.8824 precision, 0.7595 recall, and 0.8169 F1 score for bumps, and a 0.8821 precision, 0.9274 recall, and 0.9041 F1 score for normal roads. Finally, it obtained a 0.8507 precision, 0.8382 recall, and 0.8444 F1 score for the potholes. The classification performance of the SVM model with five features was inferior to that of the SVM model with four features. A receiver operating characteristic (ROC) curve, a visual graph showing the performance of a classification model at all classification threshold, was also used to further evaluate the classification performance. For example, the ROC curves for nonlinear SVM (4-features) converged closer to 1, and the area under the curve (AUC) also approached 1, as shown in Figure 16, indicating that the model did not overfitting. The algorithm also demonstrated low latency suitable for real-time applications. The processing speed was sufficient to detect and classify road hazards promptly, ensuring timely responses during the demonstration. The average success of classification was also scored by 90% for validation data sets. The proposed SVM model demonstrates high accuracy in classifying normal road surfaces, potholes and speed bumps, indicating the potential for further accuracy improvement, particularly for speed bumps via additional data acquisition and training. Future work will focus on precisely quantifying the latency to provide a more detailed analysis of the real-time performance. Our new road hazard classification system coded into Python language will be advanced for real time road hazard information system and integrated with built-in fleet management service (FMS).

IV. CONCLUSION

In this study, we have successfully developed a new passive type indirect road hazard detection and classification method based on rack force estimation of EPS systems. The main contributions are summarized as follows:

- The proposed road hazard classification method is advantageous over conventional response methods (e.g., G-sensors in suspension systems) because the signal signature obtained from estimated rack force responses is more prominent and insensitive to normal road surface characteristics.
- Combining the proposed method with cloud computing exhibits a high potential for improved accuracy. Additional training data can be accumulated over time using the cloud computing system to store road hazard information.
- Another advantage of the proposed method using an estimator (KF-UI) compared with conventional methods (response type) is that only two pieces of sensor information (steering torque and angle) are employed via the CAN bus, and the response time is relatively fast.

However, the robustness of the proposed algorithm needs further improvement against noise and parametric uncertainties. In future studies, we plan to address some of these ongoing issues. For example, we will consider the nonlinearity arising from factors such as pneumatic tire, geometric error etc. In particular, it is necessary to analyze the robustness of the SVM model against uncertainties. Our future work will focus on advancing road hazard detection and classification algorithms by incorporating additional data from smart tire sensors. This will improve the reliability and robustness of the proposed method based on the EPS system. Although our study demonstrated that the SVM model is promising to classify road hazards, some technical limitations are expected and should be further investigated. First of all, the SVM classification model may lead to degraded performance when it fits an actual response variable outside the ranges (e.g. different vehicle speeds) because most neural network-based learning models are fit to a response variable within a trained range. Therefore, the extrapolation capability of the SVM model should be accordingly further examined and improved by using more advanced classification algorithms. Next, this initial study presented a preliminary investigation on a classification method aimed at distinguishing road hazard (rectangular-shaped potholes) from normal and standard bump. However, road hazards encompass various dangers encountered while driving: irregular-shaped potholes, illegal speed bumps, road imperfections such as cracks. Accordingly, the SVM model fitted to a response variable within a trained range by only rectangular-shaped potholes may lead to degraded classification performance when it fits a different response variable outside the ranges by different road hazards such as irregular-shaped potholes. In the same context, the extrapolation capability of the SVM model should be accordingly further examined. Although our results indicate that the SVM model

is promising to classify road hazards, possible reasons remain to be discovered and could be improved by using more advanced classification algorithms.

ACKNOWLEDGMENT

The authors would like to thank the engineer Jae-In Paik and Dr. Kwang-Ki Jeon (Korea Automotive Technology Institute) for his assistance with the in-vehicle data.

REFERENCES

[1] J. Wu, H. Zhou, Z. Liu, and M. Gu, "Ride comfort optimization via speed planning and preview semi-active suspension control for autonomous vehicles on uneven roads," *IEEE Trans. Veh. Technol.*, vol. 69, no. 8, pp. 8343–8355, Aug. 2020.

[2] J. Dib, K. Sirlantzis, and G. Howells, "A review on negative road anomaly detection methods," *IEEE Access*, vol. 8, pp. 57298–57316, 2020.

[3] S. Liu, L. Zhang, J. Zhang, J. Wang, and C. Ren, "Cooperative control of path tracking and driving stability for intelligent vehicles on potholed road," *IEEE Trans. Intell. Vehicles*, vol. 9, no. 1, pp. 2499–2508, Jan. 2023.

[4] A. Dhiman and R. Klette, "Pothole detection using computer vision and learning," *IEEE Trans. Intell. Transp. Syst.*, vol. 21, no. 8, pp. 3536–3550, Aug. 2020.

[5] Y.-M. Kim, Y.-G. Kim, S.-Y. Son, S.-Y. Lim, B.-Y. Choi, and D.-H. Choi, "Review of recent automated pothole-detection methods," *Appl. Sci.*, vol. 12, no. 11, p. 5320, May 2022.

[6] R. Fan, U. Ozgunalp, B. Hosking, M. Liu, and I. Pitas, "Pothole detection based on disparity transformation and road surface modeling," *IEEE Trans. Image Process.*, vol. 29, pp. 897–908, 2020.

[7] P. M. Harikrishnan and V. P. Gopi, "Vehicle vibration signal processing for road surface monitoring," *IEEE Sensors J.*, vol. 17, no. 16, pp. 5192–5197, Aug. 2017.

[8] E. A. Martinez-Ríos, M. R. Bustamante-Bello, and L. A. Arce-Sáenz, "A review of road surface anomaly detection and classification systems based on vibration-based techniques," *Appl. Sci.*, vol. 12, no. 19, p. 9413, Sep. 2022.

[9] B. Zhou, W. Zhao, W. Guo, L. Li, D. Zhang, Q. Mao, and Q. Li, "Smartphone-based road manhole cover detection and classification," *Autom. Construct.*, vol. 140, Aug. 2022, Art. no. 104344.

[10] M. Park, Y. Jeong, and S. Yim, "Design of a modal controller with simple models for an active suspension system," *IEEE Access*, vol. 10, pp. 65585–65597, 2022.

[11] D. Chen, N. Chen, X. Zhang, and Y. Guan, "Real-time road pothole mapping based on vibration analysis in smart city," *IEEE J. Sel. Topics Appl. Earth Observ. Remote Sens.*, vol. 15, pp. 6972–6984, 2022.

[12] A. Allouch, A. Koubâa, T. Abbes, and A. Ammar, "RoadSense: Smartphone application to estimate road conditions using accelerometer and gyroscope," *IEEE Sensors J.*, vol. 17, no. 13, pp. 4231–4238, Jul. 2017.

[13] D. Jung and S. Kim, "A novel control strategy of crosswind disturbance compensation for rack-type motor driven power steering (R-MDPS) system," *IEEE Access*, vol. 10, pp. 125148–125166, 2022.

[14] Z. Liu, S. Cheng, X. Ji, L. Li, and L. Wei, "A hierarchical anti-disturbance path tracking control scheme for autonomous vehicles under complex driving conditions," *IEEE Trans. Veh. Technol.*, vol. 70, no. 11, pp. 11244–11254, Nov. 2021.

[15] A. T. Inallu, "Design of steering wheel force feedback system with focus on lane keeping assistance applied in driving simulator," M.S. thesis, Dept. Electron. Commun. Eng., Chalmers Univ. Technol., Göthenburg, Sweden, 2014.

[16] A. Bhardwaj, D. Slavin, J. Walsh, J. Freudenberg, and R. B. Gillespie, "Rack force estimation for driving on uneven road surfaces," *IFAC-PapersOnLine*, vol. 53, no. 2, pp. 14426–14431, 2020.

[17] E. Ghahremani and I. Kamwa, "Dynamic state estimation in power system by applying the extended Kalman filter with unknown inputs to phasor measurements," *IEEE Trans. Power Syst.*, vol. 26, no. 4, pp. 2556–2566, Nov. 2011.

[18] S. J. Im, J. S. Oh, and G.-W. Kim, "Simultaneous estimation of unknown road roughness input and tire normal forces based on a long short-term memory model," *IEEE Access*, vol. 10, pp. 16655–16669, 2022.

[19] S. Pan, P. Du, Y. Li, Z. Chen, and H. Wang, "The study on an general Kalman filter with unknown inputs," in *Proc. 11th World Congr. Intell. Control Autom.*, Jun. 2014, pp. 3562–3567.

[20] *CarSim (V 9.0) Reference Manual*, Mech. Simul. Corp., Ann Arbor, MI, USA, 2006.

[21] H. Guo, Z. Yin, D. Cao, H. Chen, and C. Lv, "A review of estimation for vehicle tire-road interactions toward automated driving," *IEEE Trans. Syst., Man, Cybern., Syst.*, vol. 49, no. 1, pp. 14–30, Jan. 2019.

[22] G.-W. Kim, S.-W. Kang, J.-S. Kim, and J.-S. Oh, "Simultaneous estimation of state and unknown road roughness input for vehicle suspension control system based on discrete Kalman filter," *Proc. Inst. Mech. Eng. D, J. Automobile Eng.*, vol. 234, no. 6, pp. 1610–1622, May 2020.

[23] G. O. Fosu, J. M. Opong, B. E. Owusu, and S. M. Naandam, "Modeling road surface potholes within the macroscopic flow framework," *Math. Appl. Sci. Eng.*, vol. 3, no. 2, pp. 106–118, May 2022.

[24] G.-W. Kim, "Road pothole detection based on rack force estimation of electric power steering system," presented at the FISITA World Congr., 2023.

[25] L. Nehaoua, M. Djemaï, and P. Pudlo, "Rack force feedback for an electrical power steering simulator," in *Proc. 20th Medit. Conf. Control Autom. (MED)*, Jul. 2012, pp. 79–84.

[26] E. A. Butcher, J. Wang, and T. A. Lovell, "On Kalman filtering and observability in nonlinear sequential relative orbit estimation," *J. Guid., Control, Dyn.*, vol. 40, no. 9, pp. 2167–2182, Sep. 2017.

[27] Y. Seo, K. Cho, and K. Nam, "Integrated yaw stability control of electric vehicle equipped with front/rear steer-by-wire systems and four in-wheel motors," *Electronics*, vol. 11, no. 8, p. 1277, Apr. 2022.

[28] T. Weiskircher, S. Fankem, and B. Ayalew, "Rack force estimation for electric power steering," in *Proc. Int. Design Eng. Tech. Conf. Comput. Inf. Eng. Conf.* New York, NY, USA: American Society of Mechanical Engineers, Aug. 2015, Art. no. V003T01A007.

[29] T. Abe, Y. Fujimura, T. Hirose, S. Hashimoto, M. Kajitani, K. Sato, and K. Gonpei, "Electric power steering system design based on linear quadratic control," *J. Technol. Social Sci.*, vol. 1, no. 2, pp. 37–46, 2017.

[30] W. Zhu, J. Hou, Z. Liu, and Z. Ding, "GPS positioning error compensation based on Kalman filtering," *J. Phys., Conf. Ser.*, vol. 1920, no. 1, May 2021, Art. no. 012088.

[31] M. Nachtsheim, J. Ernst, C. Endisch, and R. Kennel, "Performance of recursive least squares algorithm configurations for online parameter identification of induction machines in an automotive environment," *IEEE Trans. Transport. Electrific.*, vol. 9, no. 3, pp. 4236–4254, Sep. 2023.

[32] S. Ghosh, A. Dasgupta, and A. Swetapadma, "A study on support vector machine based linear and non-linear pattern classification," in *Proc. Int. Conf. Intell. Sustain. Syst. (ICISS)*, Feb. 2019, pp. 24–28.

[33] A. Anaissi, N. L. D. Khoa, T. Rakotoarivelo, M. M. Alamdari, and Y. Wang, "Smart pothole detection system using vehicle-mounted sensors and machine learning," *J. Civil Struct. Health Monit.*, vol. 9, no. 1, pp. 91–102, Feb. 2019.

[34] *MATLAB Statistics and Machine Learning Toolbox User's Guide*, Mathworks, Natick, MA, USA, 2022.

[35] O. Colliot, *Machine Learning for Brain Disorders*. New York, NY, USA: Springer, 2023, pp. 42–48.

[36] A. Bhardwaj, D. Slavin, J. Walsh, J. Freudenberg, and R. B. Gillespie, "Estimation and decomposition of rack force for driving on uneven roads," *Control Eng. Pract.*, vol. 114, Sep. 2021, Art. no. 104876.

HEE-BEOM LEE received the B.S. and M.S. degrees in mechanical engineering from Control Systems and Mechatronics Laboratory, Inha University, Incheon, South Korea, in 2021 and 2023, respectively. He is a Research Engineer at HL Mando Corporation. His research interests include Kalman filters, parameter estimation, vehicle control, and their industrial applications.

HO-JONG LEE received the Ph.D. degree in mechanical engineering from Virginia Polytechnic Institute and State University, USA, in 2017. He is currently with the R&D Center of HanKook Tire & Technology as the Team Leader. His research interests include tire status estimations based on smart tire sensors and application solutions using them.

KYUNG-JIN KIM received the B.S. degree in mechanical engineering from Kunsan National University, Gunsan-si, South Korea, in 2016. He is currently pursuing the M.S. degree. He is also with The Test and Certification Technology Department, Korea Automotive Technology Institute, focusing on tire testing and evaluation.

DOO-HYUN LEE received the B.S. degree in mechanical engineering from Hanyang University (ERICA), Ansan-si, South Korea, in 2021. He is currently pursuing the M.S. degree with the Control Systems and Mechatronics Laboratory, Inha University. His research interest includes Kalman filters.

GI-WOO KIM (Member, IEEE) received the Ph.D. degree from the Mechanical Engineering Department, The Pennsylvania State University, USA, in 2009. He held positions with the Powertrain R&D Center, Hyundai Motor Company, from 1996 to 2004, and the Mechanical Engineering Department, University of Michigan, from 2009 to 2011. Following this, he was an Assistant Professor with Kyungpook National University, from 2011 to 2015. From September 2015 to February 2021, he was an Associate Professor with Inha University, where he has been a Professor, since March 2021. His research interests include data-driven mechanical engineering, machine learning, measurement and control, vehicular electronics, and related fields.

• • •